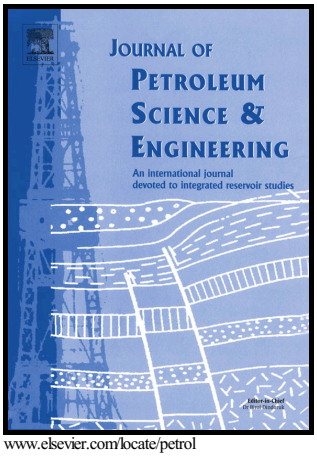

www.elsevier.com/locate/petrol

Interpretation of Two-Phase Relative Permeability Curves through Multiple Formulations and Model Quality Criteria

Leili Moghadasi, Alberto Guadagnini, Fabio Inzoli, Martin Bartosek

PII: S0920-4105(15)30153-4
DOI: http://dx.doi.org/10.1016/j.petrol.2015.10.027
Reference: PETROL3220

To appear in: *Journal of Petroleum Science and Engineering*

Received date: 4 May 2015
Revised date: 17 July 2015
Accepted date: 21 October 2015

Cite this article as: Leili Moghadasi, Alberto Guadagnini, Fabio Inzoli and Martin Bartosek, Interpretation of Two-Phase Relative Permeability Curves through Multiple Formulations and Model Quality Criteria, *Journal of Petroleum Science and Engineering,* http://dx.doi.org/10.1016/j.petrol.2015.10.027

Interpretation of Two-Phase Relative Permeability Curves through Multiple Formulations and Model Quality Criteria

Leili Moghadasi[(1)*], Alberto Guadagnini[(2, 3)], Fabio Inzoli[(1)], Martin Bartosek[(4)]

[(1)] Department of Energy, Politecnico di Milano, Via Lambruschini 4, 20156 Milano, Italy

[(2)] Department of Civil and Environmental Engineering, Politecnico di Milano, Piazza Leonardo da Vinci 32, 20133 Milano, Italy

[(3)] Department of Hydrology and Water Resources, The University of Arizona, Tucson, AZ, 85721, USA

[(4)] Eni Exploration & Production, Petroleum Engineering Laboratories, 20097 Milan, Italy.

* Corresponding author. Tel. +39 02 2399 3826. Fax. +39 02 2399 3913;

E-mail address: leili.moghadasi@polimi.it

Abstract

We illustrate the way formal model identification criteria can be employed to rank and evaluate a set of alternative models in the context of the interpretation of laboratory scale experiments yielding two-phase relative permeability curves. We consider a set of empirical two-phase relative permeability models (i.e., Corey, Chierici and LET) which are typically employed

in industrial applications requiring water/oil relative permeability quantifications. Model uncertainty is quantified through the use of a set of model weights which are rendered by model posterior probabilities conditional on observations. These weights are then employed to (*a*) rank the models according to their relative skill to interpret the observations and (*b*) obtain model averaged results which allow accommodating within a unified theoretical framework uncertainties arising from differences amongst model structures. As a test bed for our study, we employ high quality two-phase relative permeability estimates resulting from steady-state imbibition experiments on two diverse porous media, a quartz Sand-pack and a Berea sandstone core, together with additional published datasets. The parameters of each model are estimated within a Maximum Likelihood framework. Our results highlight that in most cases the complexity of the problem appears to justify favoring a model with a high number of uncertain parameters over a simpler model structure. Posterior probabilities reveal that in several cases, most notably for the assessment of oil relative permeabilities, the weights associated with the simplest models is not negligible. This suggests that in these cases uncertainty quantification might benefit from a multi-model analysis, including both low- and high-complexity models. In most of the cases analyzed we find that model averaging leads to interpretations of the available data which are characterized by a higher degree of fidelity than that provided by the most skillful model.

Keywords: Model identification criteria. Uncertainty. Two-phase relative permeability curves. Posterior probabilities.

1. Introduction

Relative permeabilities are key rock-fluid properties required for continuum-scale modeling of multiphase flow dynamics in porous and fractured media. A reliable characterization of these quantities, including proper quantification of estimation uncertainty, enables us to assess reservoir performance, forecast ultimate oil recovery, and investigate the efficiency of enhanced oil recovery techniques. In this broad context, we focus here on laboratory-scale relative permeabilities associated with two-phase fluid flow. Acquisition of accurate relative permeability data is of critical importance and has always been of central interest in the oil industry (Silpngarmlers et al., 2002) where formulations based on analogies to Darcy's Law are routinely employed to model multiphase flow. Core flooding experiments represent the main approach to determine two-phase relative permeabilities. The latter are typically estimated upon relying on empirical correlations/models. Relative permeability curves, depicting the (typically nonlinear) dependence of relative permeability on fluid phase saturation, are then employed to simulate two-phase flow under desired field settings. Two-phase information of this kind are also employed to estimate three-phase relative permeabilities on the basis of a set of pseudo-empirical models (e.g., Ranaee et al., 2015 and references therein).

A variety of experimental techniques are available for the assessment of two-phase relative permeability curves (Botermans et al., 2001; Feigl, 2011; Firoozabadi and Aziz, 1991; Liu et al., 2010; Toth et al., 2002). The two types of laboratory settings which are usually considered are associated with (*i*) steady-state (SS), or (*ii*) unsteady-state (US) conditions. Relative permeability estimates may also be obtained from field data upon relying on the production history of a reservoir, its geological makeup and its fluid properties. This approach is conducive to effective / equivalent macroscopic parameters. The way laboratory scale values can be transferred to field scale settings is still a challenging area of research.

Laboratory characterization of two-phase relative permeability through either steady- or unsteady-state methods can be expensive and time consuming. Steady-state techniques consider simultaneous injection of the two phases in a rock core. A given total fluid flow rate is typically imposed and diverse fractional flow rates are considered for each phase. Measurements of total pressure drop, fluid flow rates and fluid flow saturations in the sample are then taken after steady-steady state conditions are attained. Experimental data are then interpreted through a selected model, leading to estimates of two-phase relative permeabilities within a relatively broad range of saturation values. A key drawback of the technique is associated with the typically long times associated with the attainment of steady-state (Cao et al., 2014; Honarpour et al., 1986; Kikuchi et al., 2005).

Unsteady-state methods consider injection of only one of the phases in the core. The latter is saturated with the displaced phase, the displacing phase being at irreducible saturation. Phase recovery and pressure drop across the core are continuously recorded during the displacement process. The approach is efficient in terms of execution time but leads to estimates of two-phase relative permeabilities in a narrow saturation range, usually grouped towards the high end of wetting phase saturation values (Ebeltoft et al., 2014; Sylte et al., 2004).

Measurements of relative permeabilities can be employed to test the reliability of a given conceptual structure and mathematical formulation of an interpretive model. The reliability of model predictions depends on the way the model structure is defined and on the degree of fidelity associated with model parametrization. Empirical models which are most frequently employed to interpret experimentally determined two-phase relative permeability curves through model parameter estimation include (*a*) the Corey formulation (Corey, 1954), (*b*) the models proposed by Sigmund & McCaffery (Sigmund and McCaffery, 1979) and Chierici (Chierici,

1984), and (*c*) the recent LET model (Ebeltoft et al., 2014; Lomeland et al., 2005). Interpretation of laboratory measurements through these empirical models may provide relative permeabilities for a limited range of saturations. This is mainly due to hypotheses and heuristic concepts associated with most of the available empirical models, which might render them unsuitable to match laboratory data for the whole range of saturations.

Notable weak points of available studies are that they (*a*) either rely on a single mathematical model depicting the two-phase flow processes, or (*b*) analyze alternative mathematical formulations through criteria such as least-square regression (e.g., Lomeland et al. 2005, and Ebeltoft et al., 2014) which do not provide rigorous information about the way diverse models can be ranked and/or employed in a multi-model modeling framework. Yet, it is known that multi-phase flow processes and the porous media hosting them are remarkably complex. As a consequence, observations are amenable to be interpreted through various mathematical formulations, each requiring an appropriate parametrization. This aspect can be assessed through Model Quality criteria employed within a Maximum Likelihood theoretical approach. This allows considering the effects of conceptual model uncertainty on parameter estimation and provides theoretically robust guidance in the model selection process. In this context, a multi-model analysis based on averaging the responses of diverse models can be a powerful tool to naturally accommodate existing differences amongst models within a unique theoretical framework (Lu, 2012). Benefits of the approach have been exposed in the context of diverse environmental systems, including groundwater flow settings (e.g., Carrera and Neuman, 1996; Ye et al., 2004; Ye et al., 2008; Riva et al., 2009; Riva et al., 2011 and references therein), as well as in the interpretation of complex competitive sorption reactive processes in natural soils (Bianchi Janetti et al., 2012).

To the best of our knowledge, analyses of applications of this methodology to the interpretation of multiphase flow process are still lacking. Here, we illustrate the way Maximum Likelihood parameter estimation and model identification criteria associated with a multi-model framework can be jointly employed on a set of laboratory scale experiments involving steady-state two-phase flow of oil and water in two cores, a quartz Sand-pack and a Berea sandstone. We then apply the approach to reassess the interpretation of a series of published data-sets. We do so by (*a*) considering and comparing the performances of three commonly employed empirical models, i.e., the Corey (Corey, 1954), Chierici (Chierici, 1984), and LET (Ebeltoft et al., 2014; Lomeland et al., 2005) models, (*b*) quantifying the uncertainty associated with each of these models, and (*c*) illustrating the ability of a model averaging (MA) approach to interpret the available data when compared against the results provided by the model with the highest rank in the model set considered.

2. Materials and Methods

2.1 Experimental Setup and Data Analyzed

This section provides a brief description of our experimental setup and technical aspects of measurement procedures. Figure 1a depicts a sketch of the setup. The latter comprises (a) Hassler-type core holders (TEMCO FCH-1.5m) containing the tested rock samples, (b) an X-Ray saturation monitoring equipment (Core Lab Instruments - Reservoir Optimization), and (c) a close loop pumping system. The experiments are performed on two porous media, i.e., a column of quartz Sand-pack and a water-wet Berea sandstone core. Each of the samples is placed inside a rubber sleeve with inner diameter of 0.0381 m and length of 0.30 m. The fluids employed in the displacement experiments are distilled water and isoparaffinic mineral oil. Table 1 lists the characteristics of the core samples and of the fluids. The flowing water is tagged with X-ray

absorbing chemicals (NaBr for the Sand-pack and KBr for the Berea core sample) to increase X-ray attenuation coefficient and improve measurement accuracy.

Two-phase relative permeabilities associated with continuum (Darcy) scale characterization of water and oil displacement in the samples have been estimated under steady-state (SS) conditions. We performed SS imbibition experiments, each characterized by a given ratio between the flow rates of oil and water. The fluids are jointly injected in the system following the sequence depicted in Fig.1b. (Step *A*).

Absolute permeability to water has been measured by a first set of experiments performed by applying a sequence of diverse flow rates and employing Darcy's law. The imbibition experiments started after full saturation of the rock sample with water. The system has been sustained for 24 h under these fully saturated conditions to ensure equilibrium (Step *A* in Fig. 1b). X-ray saturation measurements are performed during this phase to achieve proper calibration against water content. An oil imbibition phase with water displacement is then started. Oil injection takes place until no more water is eluted from the system. Irreducible water saturation (S_{wi}) is then measured (Step *B* in Fig. 1b) and oil absolute permeability at irreducible water saturation, $K_{o(Swi)}$, is assessed for these conditions.

A collection of experiments consisting of joint injection of oil and water is then performed. We do so upon setting a total constant flow rate of 480 [ml/h] and 30 [ml/h], respectively for the Sand-pack and the Berea cores, and increasing water fractional flow while decreasing oil fractional flow (Steps *C*-*E* in Fig. 1b).

X-ray scans provide longitudinal (depth-average) saturation profiles of oil and water along the core. For a given fractional flow, measurements of pressure drop across the core and depth-averaged saturation profiles are taken at steady-state, i.e., when no appreciable changes of

pressure drop and saturation profiles are observed. Note that attaining equilibrium (i.e., steady-state) for each of these steps requires (approximately) one day. Residual oil saturation (S_{or}) is established at the end of the sequence of imbibition processes, when no more oil is produced from the system (Step *F* in Fig. 1b). Three replicates of each experiment have been performed. After finishing each step and before starting a new test, the core sample was cleaned and washed. We then measured again absolute permeability and pore volume / porosity. For all our experiments, these quantities did not show detectable changes with respect to the values measured at the beginning of the test.

Relative permeabilities are calculated starting from the application of the classical Darcy-scale expressions

$$K_o = \frac{q_o \mu_o l}{A(\Delta p_o)} \; ; \qquad K_w = \frac{q_w \mu_w l}{A(\Delta p_w)} \tag{1}$$

Here, K_o [L^2] and K_w [L^2] are absolute oil and water permeability; q_o and q_w are volumetric flow rates [L^3 T^{-1}] for oil and water, respectively; μ_o and μ_w [M L^{-1} T^{-1}] respectively are dynamic viscosity of oil and water; A [L^2] and l [L] are core cross-sectional area and length; $\Delta p_o = \Delta p_w = \Delta p_{core}$ [M L^{-1} T^{-2}] is pressure drop between inlet and outlet of the core. Relative permeabilities, respectively denoted as K_{ro} and K_{rw} for water and oil, are expressed with respect to oil permeability at irreducible water saturation, $K_{o(Swi)}$, i.e.,

$$K_{ro} = \frac{K_o}{K_{o(Swi)}} ; \qquad K_{rw} = \frac{K_w}{K_{o(Swi)}} \tag{2}$$

We also consider in our analysis two datasets presented by Lomeland et al. (2005) and related to steady-state experiments performed at reservoir conditions on core samples from the Norwegian Continental Shelf. These are the results of SS experiments performed on core samples with lengths of 0.31 m and 0.12 m, respectively. For ease of reference, these two

datasets are hereinafter termed as "D1" and "D2". Table 2 lists core sample and fluid properties associated with these experiments. Lomeland et al. (2005) proposed a three-parameter model to interpret the inferred two-phase relative permeability curves (see Section 2.2.3 for a brief description of their model).

2.2 Two-phase relative permeability models

Several empirical formulations are available to characterize observed water-oil relative permeability curves (Al-Fattah, 2003; Chierici, 1984; Corey, 1954; Honarpour et al., 1982; Lomeland et al., 2005). The structure of these models is typically driven by experimental observations, theoretical arguments and / or heuristic concepts. Each model is associated with a set of parameters which are usually estimated through fits against experiments, i.e., against available relative permeability curves. We provide in the following a brief overview of the models we consider in this work.

2.2.1 Corey Model

The Corey model (Corey, 1954) is usually employed due to its simplicity, the limited amount of input data requirements, and the small number of parameters to be estimated. The mathematical structure of the model rests on capillary pressure concepts and is widely accepted to be fairly accurate for consolidated porous media (Honarpour et al., 1986). The model has also been proposed for unconsolidated sands through proper tuning of its parameters. Corey's equations for wetting (water) and non-wetting (oil) relative permeability read

$$K_{rw} = K_{rw}^{o}(S_w^*)^{N_w} \tag{3}$$

$$K_{ro} = K_{ro}^{w}(1-S_w^*)^{N_o} \tag{4}$$

$$S_w^* = \frac{S_w - S_{wi}}{1-S_{wi}-S_{or}} \tag{5}$$

Here, K_{rw} and K_{ro} respectively are the water and oil phase relative permeabilities; S_w^* is normalized water saturation; K_{rw}^0 and K_{ro}^0 respectively are the end-points of water and oil relative permeability curves; N_w and N_o are parameters to be estimated through model calibration. These parameters drive the curvature of the relative permeability curves.

2.2.2 Chierici Model

Chierici (Chierici, 1984) proposed the following exponential formulations for water-oil imbibition relative permeability curves

$$K_{rw} = K_{rw}^o e^{-B\left(\frac{S_w - S_{wi}}{1 - S_{or} - S_w}\right)^{-M}} \tag{6}$$

$$K_{ro} = K_{ro}^w e^{-A\left(\frac{S_w - S_{wi}}{1 - S_{or} - S_w}\right)^{L}} \tag{7}$$

Typically, S_{wi}, S_{or}, K_{rw}^o and K_{ro}^w are observed, while the model parameters B, M, A and L are estimated through model calibration (Chierici, 1984; Chierici, 1994; Sylte et al., 2004).

These formulations provide a reasonably good match against experimental relative permeability curves. They are considered to provide improved approximations at and near the initial and end points of these curves when compared against the Corey model and other polynomial approximations (Feigl, 2011). The flexibility of the model is mainly due to the possibility of representing concave and/or convex relative permeability curves as a function of parameter values.

2.2.3 LET Model

LET was proposed as a new versatile model (Lomeland et al., 2005). It is expressed in the form

$$K_{rw} = K_{rw}^{o} \frac{(S_w^*)^{L_w}}{(S_w^*)^{L_w} + E_w(1-S_w^*)^{T_w}} \tag{8}$$

$$K_{ro} = K_{ro}^{w} \frac{(1-S_w^*)^{L_o}}{(1-S_w^*)^{L_o} + E_o(S_w^*)^{T_o}} \tag{9}$$

Here, model parameters are L_i, E_i, and T_i (i = w, o). Values of T_i and L_i respectively drive the shape of the lower and upper part of the relative permeability curve, while E_i describes the slope and the elevation of the central portion of the curve. As such, the model is designed to include diverse parts of the relative permeability curve to capture variable behavior across the entire saturation range (Ebeltoft, 2014; Lomeland et al., 2005; Sendra, 2013). The model has been shown to provide good interpretation of experimental data over a considerable range of oil saturations.

2.3 Maximum Likelihood Parameter Estimation and Model Quality Criteria

This section briefly outlines the approach and algorithms employed in the parameter estimation procedure and some implementation details. Parameter estimation is performed in the typical Maximum Likelihood (ML) framework.

Let us denote with N_K the number of available observation data (i.e., the number of two-phase relative permeability data), the N_p as the number of unknown model parameters and $\mathbf{P}$ as a vector of unknown model parameters $\mathbf{P} = \left[P_1, P_2, ..., P_{N_p} \right]$.

We consider $\mathbf{K}^* = \left[K_1^*, K_2^*, ..., K_{N_K}^* \right]$ and $\hat{\mathbf{K}} = \left[\hat{K}_1, \hat{K}_2, ..., \hat{K}_{N_K} \right]$ to be vectors respectively collecting the set of N_K available relative permeability observations and model predictions at the corresponding fluid saturations. ML estimates $\hat{\mathbf{P}} = \left[\hat{P}_1, \hat{P}_2, ..., \hat{P}_{N_p} \right]$ of the elements of $\mathbf{P} = \left[P_1, P_2, ..., P_{N_p} \right]$ for a given model can be estimated through minimization, with

respect to **P**, of the negative log likelihood criterion (e.g., Carrera and Neuman, 1986; Bianchi Janetti et al., 2012 and references therein)

$$NLL = \sum_{i=1}^{N_K} \frac{J_i}{\sigma_i^2} + \ln\left|\mathbf{B}_K\right| + N_K \ln(2\pi) \tag{10}$$

where $J_i = (K_i^* - \hat{K}_i)^2$ and $\mathbf{B}_K$ is the covariance matrix of measurement errors, here considered to be diagonal with non-zero terms equal to the observation error variance σ_i^2 (Carrera and Neuman, 1986). Minimization of (10) is achieved through the iterative Levenberg-Marquardt algorithm as embedded in the public domain code PEST (Doherty, 2013).

When N_M multiple models are considered for the interpretation of the physical scenario of interest, one may minimize (10) for each model formulation. In this case, once the parameters associated with each model are estimated, the N_M alternative formulations can be ranked by various criteria (e.g., Neuman, 2003; Ye et al., 2004, 2008; Neuman et al., 2011; Bianchi Janetti et al., 2012 and references therein), including

$$AIC = NLL + 2N_P, \tag{11}$$

$$AIC_c = NLL + 2N_P + \frac{2N_P(N_P+1)}{N_K - N_P - 2}, \tag{12}$$

$$BIC = NLL + N_P \ln(N_K), \tag{13}$$

$$KIC = NLL - N_K \ln(2\pi) - \ln\left|\mathbf{Q}\right| \tag{14}$$

Here, the Akaike information criterion, *AIC*, is due to Akaike (Akaike, 1974), AIC_c to Hurvich and Tsai (Hurvich and Tsai, 1989), *BIC* to Schwartz (Schwarz, 1978) and *KIC* to Kashyap (Kashyap, 1982). In (14), **Q** is the Cramer-Rao lower-bound approximation for the covariance matrix of parameter estimates (see Ye et al., 2008 for details). Models associated with smaller values of a given criterion are ranked higher than those associated with larger values. As shown

by, e.g., Hernandez et al. (2006), Ye et al. (2008), and Riva et al. (2011), it can be noted that *KIC* tends to favor models with relatively small expected information content per observation, when one considers models associated with the same number of parameters, equal minima of *NLL*, and the same prior probability linked to parameter values linked to *NLL* minimum.

The values of a given discrimination criterion associated with model M_K can be translated into a posterior model weight, $P(M_K|K^*)$, which can be employed to quantify uncertainty. This posterior probability can be computed according to (Ye et al., 2008)

$$P(M_K|K^*)=\frac{\exp(-\frac{1}{2}\Delta IC_K)P(M_K)}{\sum_{i=1}^{N_M}\exp(-\frac{1}{2}\Delta IC_i)P(M_i)}, \quad (15)$$

Here, $\Delta IC_K = IC_K - IC_{\min}$, IC_K being any of the model discrimination criteria (11)-(14), and $IC_{\min}$ is the minimum value of IC_K over these models; $P(M_k)$ is the prior probability of model M_k. We consider $P(M_k) = 1 / N_M$ if no prior information is available, assigning equal prior probability to each model. In the following we employ the above introduced model identification criteria and posterior model probabilities to rank the tested two-phase permeability (water-oil) models.

Model average (MA) can then be calculated by weighting each model through its posterior probability (Ye et al., 2010). The skill of each model and of MA results to interpret the observed data is compared through the following two metrics, i.e., the Normalized Mahalanobis Distance, *NMD* (Winter 2010 and references therein), and the traditional Mean Square Error, *MSE*. The *NMD* is a generalized distance which was first introduced to assess the degree of similarity between two different populations and is defined as

$$NMD(\mathbf{K}^*, \hat{\mathbf{K}})=\sqrt{(\mathbf{K}^*-\hat{\mathbf{K}})^T\mathbf{S}^{-1}(\mathbf{K}^*-\hat{\mathbf{K}})+\log|\mathbf{S}|} \quad (16)$$

S being the ($N_P \times N_P$) covariance matrix corresponding to the data points and $|\mathbf{S}|$ its determinant. The first term appearing on the right hand side of (16) is the square of the Mahalanobis Distance (Mahalanobis 1936), the second term acting as a regularization quantity. As noted by Winter (2010), the *NMD* has the same structure of (10) up to a constant which does not influence on model comparison. The use of *MSE* is based on the observation that it is arguably the simplest and most common criterion employed to evaluate the performance of an estimator and its use in comparisons of the relative performance and accuracy of each model and the resulting MA results is well documented, e.g., in the context of regional climate model data (Winter and Nychka, 2010).

3. Results and discussion

Here we illustrate our experimental results detailing the relative permeability curves obtained through SS imbibition experiments on Sand-pack and Berea sandstone cores. We then present our ML model calibration results based on our data and datasets D1 and D2 illustrated in Section 2.1.

3.1 Experimental results

Figure 2 depicts the dependence of the relative permeability imbibition versus core saturation obtained from X-ray in-situ measurements for the tested core samples. Three replicates have been conducted for each experiment, as detailed in Appendix A, and each point in Figure 2 represents the average of the three experiments performed (see also Figures A1 and A2 for the depiction of the complete dataset). Table A1 lists average values of relative

permeabilities and water saturation together with the associated estimate of standard deviation, as calculated on the basis of the experimental replicates depicted in Figures A1 and A2.

Figure 2 shows that the crossover between water and oil relative permeability takes place at 77% and 60% water saturation for the Sand-pack and Berea core sample, respectively. The location of these crossing points in the water saturation space ($S_w \geq 50\%$) is consistent with an interpretation of the estimated relative permeabilities as being associated with water-wet rock conditions (Craig, 1993). It is also observed that the Sand-pack is characterized by the lowest irreducible water saturation and largest water relative permeability due to the higher connectivity of its pore space when compared to that of the sandstone core. The higher irreducible water saturation and lower water relative permeability observed for the Berea core sample are consistent with the likelihood of occurrence of significant capillarity effects and trapping of the non-wetting phase (oil) during two-phase flow conditions.

3.2 Parameter Estimation and Model Identification Criteria

Table A2 and A3 in Appendix A list the results of the calibration of the tested relative permeability models against our experimental data in terms of the estimated value of each parameter, denoted as C, the upper (U) and lower (L) limits identifying the 95% uncertainty bounds around the estimate, and the ratio $\Re = (U - L) / C$. Results associated with experiments D1 and D2 of (Lomeland et al., 2005) are also listed. Figures 3-5 illustrate graphical depictions of the estimated model parameter values for K_{rw} and K_{ro} associated with the four considered datasets and the three model analyzed. Intervals associated with U and L are also depicted. We can observe that parameter estimates linked to the Corey model are generally characterized by the smallest values of $\Re$, indicating that relatively robust estimates have been obtained.

Otherwise, the quality of the estimates of most of the LET model parameters appears to be relatively poor when analyzed in terms of this metric.

Our results show that all estimates of model parameters depend on the particular dataset employed for model calibration, the ratio between the lowest and highest estimated value of a given parameter ranging between approximately 2 and 6. Notable exception is given by E_o associated with the LET model (9) whose estimates are relatively stable across datasets (with a variability of about 35%). The values of $\Re$ tend to be generally low (less than 0.5), even as markedly varying across datasets, suggesting that in general reliable parameter estimates can be obtained for the models, albeit with some exception as noted above. Some of the LET model parameters (most notably E_i ($i = w, o$)) are linked to the largest values of $\Re$. This indicates that in some cases the complexity of the model structure might render parameter estimates associated with increased uncertainty. It has also to be noted that values of $\Re > 1$ are in some cases associated with low sensitivity of a model to a given parameter (details not shown).

Figures 6-9 provide graphical depictions of relative permeabilities K_{rw} and K_{ro} versus water saturation for the four considered datasets together with the results of all calibrated models. These results are complemented by those associated with MA analyses, performed according to the approach outlined in Section 2.3. Uncertainty bounds associated with model estimates and corresponding to Gaussian 95% confidence intervals (computed numerically by Monte Carlo sampling relying on the estimation covariance matrix of the parameters) are also depicted. It can be noted that, even as estimated K_{rw} curves rendered by the three models are virtually coinciding, the LET model allows capturing all key details embedded in the S-shape behavior of K_{ro}, including the range of values associated with low saturations (Kjosavik et al., 2002; Lake, 1986; Lomeland et al., 2005; Mian, 1992; Slider, 1983). Model identification criteria

(11)–(14) and posterior probabilities are then employed to rank each model for the datasets analyzed. Table 3 lists the results of model identification criteria associated with K_{rw} for each two-phase model and calibration set (the smallest values for each dataset are highlighted in bold). Model posterior probabilities are also included for completeness. Table 4 lists the corresponding results associated with oil relative permeability. As an example, Figures A3 and A4 in Appendix A depict model posterior probabilities calculated on the basis of *KIC*.

The adoption of model identification criteria and posterior model probabilities allows ranking of the candidate models tested on the basis of their associated posterior probabilities. Note that, as indicated in Section 2.3, the smallest value of a given model identification criterion indicates the most favored model (according to the considered criterion) at the expenses of the remaining models. A preliminary evaluation based on the identification of the smallest value of a given model identification criterion reveals that *KIC* consistently indicates the LET as the best model for all datasets. Otherwise, the other criteria considered may lead to different conclusions depending on the dataset considered.

The posterior model weights not always indicate that one model has a considerably high degree of likelihood at the expense of the remaining two, depending on the set of observations considered. For the sake of our discussion, and considering that *KIC* has been shown to be more accurate than other criteria to calculate (15) (Lu et al., 2011), we focus here on posterior weights based on *KIC* in our interpretation. Results for K_{rw} based on *KIC* indicate that the Chierici model is associated with a non-negligible weight for all datasets, the weights of the Corey model being virtually negligible. The LET model is generally linked with the highest weights. A similar pattern emerges from the analysis of K_{ro} curves, where the LET model is clearly indicated by *KIC* as the preferred model for datasets D1 and D2 and our experiments related to the Sand-pack

core, while the interpretation of the Berea dataset suggests that the Corey and Chierici models can also have a significant weight.

All these observations support the interpretation included in Figures 6-9 based on model averaging (MA) and obtained as a weighted average (through (15)) of the results associated with each individual model. A quantitative comparison of the interpretative skill of the average of the model collection to the skills of the individual members is performed through the use of the *NMD* (16) and *SME*, as illustrated in Section 2.3. Table 5 lists the average Mahalanobis distance, NMD_m, associated with K_{rw} data for each model of the population considered and its MA based counterpart together with the standard deviation of *NMD*, *SDNMD*, the resulting coefficient of variation, $CV = SDNMD / NMD_m$, and the Mean Square Error, *MSE*. The corresponding results obtained for K_{ro} are listed in Table 6. From Figures 6-9 and Tables 5 and 6 one can also observe that model averaged results lead to high fidelity representations of the experimental observations. MA results appear to be of higher quality than those obtained with the most skillful model (i.e., LET) in most cases, with particular reference to K_{ro}. These results are consistent with the observation that the model average can be more skillful than the model ranked as highest in cases where the individual models in the collection lead to data interpretations of diverse qualities.

Our results generally support the findings of Kerig and Watson (1986) and Lomeland et al. (2005) who indicated that the Corey and Chierici models are not flexible enough to reconcile the entire set of experimental observations. However, they also suggest that in some cases, most notably for the interpretation of K_{rw} data, the higher complexity of the LET model does not justify selecting it at the expenses of other, simpler models. In such scenarios, a multi-model analysis of the kind we present can be more appropriate.

4. Conclusions

We produce high quality two-phase relative permeability datasets resulting from Steady-State imbibition experiments on two diverse porous media, a quartz Sand-pack and a Berea sandstone core. The ability of three commonly employed empirical two-phase models (i.e., Corey, Chierici and LET) to capture the observed behavior has been analyzed on the basis of rigorous model identification criteria. The latter have been applied to rank the selected alternative models through (a) the identification of the smallest value of a given criterion and (b) the evaluation of weights given by posterior model probabilities, conditional on a given dataset. We estimate the parameters of each model within a Maximum Likelihood framework for our experiments as well as additional published datasets (Lomeland et al. 2005).

Our results show that the LET model, which relies on the largest number (three) of uncertain parameters, appears to exhibit sufficient flexibility to satisfactorily capture the entire set of experimental data, thus suggesting that capturing continuum scale manifestations of these complex phenomena might require considering flexible functional forms at the expenses of a high number of parameters. Model discrimination based on the smallest value of a given model identification criterion reveals that *KIC* indicates the LET as the best model for all datasets, while other criteria lead to contrasting results as a function of the dataset considered. A detailed analysis of the alternative models based on posterior (conditional) probabilities reveals that in several cases, most notably for assessment of K_{rw} curves, the weights associated with the simple Chierici and Corey models cannot be considered as negligible. In these cases, a single interpretive model such as the LET which is associated with the highest number of parameters,

might not succeed in providing a complete uncertainty quantification and a multi-model analysis, including also low-complexity models in a model averaged (MA) analysis, should be favored.

In this context, we compare the interpretative skill of the average of the model collection to the skills of the individual members on the basis of the Normalized Mahalanobis Distance and mean square error. Our study suggests that model averaged results tend to produce high fidelity representations of the experimental observations, MA results being of higher quality than those obtained with the most skillful model (i.e., LET) in most cases, with particular reference to K_{ro}.

ACKNOLWEDGMENTS

Partial financial support from Eni SpA is gratefully acknowledged.

TABLE CAPTIONS

Table 1. Physical properties of core sample and fluids.

Table 2. Physical properties of Norwegian Continental Shelf core samples and fluids for experiments D1 and D2 (Lomeland et al. 2005).

Table 3. Model Calibration and Identification Criteria and Corresponding Posterior Probability (in parenthesis) associated with K_{rw} (the smallest values for each dataset are highlighted in bold).

Table 4. Model Calibration and Identification Criteria and Corresponding Posterior Probability (in parenthesis) associated with K_{ro} (the smallest values for each dataset are highlighted in bold).

Table 5. Average Mahalanobis distance (NMD_m), standard deviation of *NMD* (*SDNMD*), the resulting coefficient of variation ($CV = SDNMD / NMD_m$) and Mean Square Error (*MSE*) for each model of the population considered and its MA-based counterpart for K_{rw}.

Table 6. Average Mahalanobis distance (NMD_m), standard deviation of *NMD* (*SDNMD*), the resulting coefficient of variation ($CV = SDNMD / NMD_m$) and Mean Square Error (*MSE*) for each model of the population considered and its MA-based counterpart for K_{ro}.

FIGURE CAPTIONS

Fig. 1. (a) Sketch of experimental set-up; (b) Steady State (SS) imbibition process.

Fig. 2. Steady-State Imbibition relative permeabilities versus average water saturation.

Fig. 3. Estimated Corey model parameter values for (a) K_{rw} and (b) K_{ro} associated with the four considered datasets. Intervals associated with the upper (U) and lower (L) limits identifying the 95% uncertainty bounds around the estimate are also depicted.

Fig. 4. Estimated Chierici model parameter values for (a) K_{rw} and (b) K_{ro} associated with the four considered datasets. Intervals associated with the upper (U) and lower (L) limits identifying the 95% uncertainty bounds around the estimate are also depicted.

Fig. 5. Estimated LET model parameter values for (a) K_{rw} and (b) K_{ro} associated with the four considered datasets. Intervals associated with the upper (U) and lower (L) limits identifying the 95% uncertainty bounds around the estimate are also depicted.

Fig. 6. Graphical depictions of (a) K_{rw}, (b) K_{ro} versus water saturation for the Sand-pack experiments together with the results of all calibrated models, uncertainty bounds corresponding to Gaussian 95% confidence intervals and model average (MA).

Fig. 7. Graphical depictions of (a) K_{rw}, (b) K_{ro} versus water saturation for the Berea sandstone experiments together with the results of all calibrated models, uncertainty bounds corresponding to Gaussian 95% confidence intervals and model average (MA).

Fig. 8. Graphical depictions of (a) K_{rw}, (b) K_{ro} versus water saturation for dataset D1 together with the results of all calibrated models, uncertainty bounds corresponding to Gaussian 95% confidence intervals and model average (MA).

Fig. 9. Graphical depictions of (a) K_{rw}, (b) K_{ro} versus water saturation for dataset D2 together with the results of all calibrated models and uncertainty bounds corresponding to Gaussian 95% confidence intervals and model average (MA).

Ethical Statement

The authors declare that they have no conflict of interest.

References

Akaike, H., 1974. A new look at the statistical model identification. Automatic Control, IEEE Transactions on, 19(6): 716-723.

Al-Fattah, S.M., 2003. Empirical Equations for Water/Oil Relative Permeability in Saudi Sandstone Reservoirs. Society of Petroleum Engineers.

Botermans, C.W., van Batenburg, D.W. and Bruining, J., 2001. Relative Permeability Modifiers: Myth or Reality? Society of Petroleum Engineers.

Cao, J., James, L.A. and Johansen, T.E., 2014. Determination of two phase relative permeability from core floods with constant pressure boundaries. International Symposium of the Society of CoreAnalysis ,Avignon, France, 8-1 September, 2014.

Chierici, G.L., 1984. Novel Relations for Drainage and Imbibition Relative Permeabilities.

Chierici, G.L., 1994. Principles of petroleum reservoir engineering.

Corey, A.T., 1954. The interrelation between gas and oil relative permeabilities. Prod, Monthly

Craig, F.F., 1993. The reservoir engineering aspects of waterflooding. Richardson, TX: Henry L. Doherty Memorial Fund of AIME, Society of Petroleum Engineers.

Ebeltoft, E., Lomeland, F., Brautaset, A. and Haugen, Å., 2014. Parameter based scal-analysing relative permeability for full field application. International Symposium of the Society of Core

Analysis,Avignon, France, 8-11 September, 2014.

Ebeltoft, F.L.E., 2014. Versatile three-phase correlations for relative permeability and capillary pressure.

Feigl, A., 2011. Treatment of relative permeabilities for application in hydrocarbon reservoir simulation model. Nafta, 62(7-8): 233-243.

Firoozabadi, A. and Aziz, K., 1991. Relative Permeabilities From Centrifuge Data.

Honarpour, M., Koederitz, L. and Harvey, A.H., 1986. Relative permeability of petroleum reservoirs. C.R.C. Press.

Honarpour, M., Koederitz, L.F. and Harvey, A.H., 1982. Empirical Equations for Estimating Two-Phase Relative Permeability in Consolidated Rock.

Hurvich, C.M. and Tsai, C.-L., 1989. Regression and time series model selection in small samples. Biometrika, 76(2): 297-307.

Kashyap, R.L., 1982. Optimal Choice of AR and MA Parts in Autoregressive Moving Average Models. IEEE Transactions on Pattern Analysis and Machine Intelligence, PAMI-4(2): 99-104.

Kikuchi, M.M., Branco, C.C., Bonet, E.J., Zanoni, R.M. and Paiva, C.M., 2005. Water Oil Relative Permeability Comparative Study: Steady Versus UnSteady State.

Kjosavik, A., Ringen, J.K. and Skjaeveland, S.M., 2002. Relative Permeability Correlation for Mixed-Wet Reservoirs.

Lake, L.W., 1986. Fundamentals of enhanced oil recovery. Society of Petroleum Engineers.

Liu, R., Liu, H., Li, X., Wang, J. and Pang, C., 2010. Calculation of Oil and Water Relative Permeability for Extra Low Permeability Reservoir. Society of Petroleum Engineers.

Lomeland, F., Ebeltoft, E. and Thomas, W.H., 2005. A new versatile relative permeability correlation, International Symposium of the Society of Core Analysts, Toronto, Canada, pp. 21-25.

Lu, D., 2012. Assessment Of Parametric And Model Uncertainty In Groundwater Modeling, Electronic Thesis, Treatises and sissertations, Paper 5003, http://diginole.lib.fsu.edu/etd/5003.

Lu, D., Ye, M. and Neuman, S., 2011. Dependence of Bayesian Model Selection Criteria and Fisher Information Matrix on Sample Size. Math Geosci, 43(8): 971-993.

Mian, M.A., 1992. Petroleum Engineering Handbook for the Practicing Engineer. PennWell Books.

Schwarz, G., 1978. Estimating the dimension of a model. The annals of statistics, 6(2): 461-464.

Sendra, 2013. User guide.

Sigmund, P. and McCaffery, F., 1979. An improved unsteady-state procedure for determining the relative-permeability characteristics of heterogeneous porous media (includes associated papers 8028 and 8777). Society of Petroleum Engineers Journal, 19(01): 15-28.

Silpngarmlers, N., Guler, B., Ertekin, T. and Grader, A.S., 2002. Development and Testing of Two-Phase Relative Permeability Predictors Using Artificial Neural Networks.

Slider, H.C., 1983. Worldwide Practical Petroleum Reservoir Engineering Methods. PennWell Books.

Sylte, A., Ebeltoft, E. and Petersen, E.B., 2004. Simultaneous Determination of Relative Permeability and Capillary Pressure Using Data from Several Experiments.

Toth, J., Bodi, T., Szucs, P. and Civan, F., 2002. Convenient formulae for determination of relative permeability from unsteady-state fluid displacements in core plugs. Journal of Petroleum Science and Engineering, 36(1–2): 33-44.

Ye, M., Meyer, P.D. and Neuman, S.P., 2008. On model selection criteria in multimodel analysis. Water Resources Research, 44(3).

Ye, M., Pohlmann, K.F., Chapman, J.B., Pohll, G.M. and Reeves, D.M., 2010. A model-averaging method for assessing groundwater conceptual model uncertainty. Groundwater, 48(5): 716-728.

Table A1. Steady-State Imbibition Relative Permeabilities (K_{rw}: oil relative permeability; K_{ro}: water relative permeability) and water saturation, S_w, for the sand-pack and the Berea

sandstone samples. Average values together with the estimated standard deviation of data are listed, as calculated on the basis of the m = 3 experimental replicates depicted in Figures A1 and A2.

Sand-pack			Berea Sandstone		
S_w	K_{rw}	K_{ro}	S_w	K_{rw}	K_{ro}
0.19±0.012	0.0	0.781±0.015	0.42±0.015	0.0	0.781±0.001
0.47±0.011	0.0086±0.011	0.47±0.009	0.54±0.012	0.015±0.00001	0.23±0.002
0.51±0.004	0.015±0.001	0.42±0.005	0.56±0.012	0.03±0.001	0.085±0.001
0.56±0.005	0.022±0.004	0.35±0.008	0.58±0.011	0.022±0.001	0.045±0.001
0.62±0.01	0.050±0.001	0.27±0.012	0.60±0.016	0.050±0.001	0.022±0.001
0.77±0.004	0.168±0.016	0.098±0.008	0.62±0.004	0.168±0.002	0.006±0.003
0.86±0.02	0.433±0.014	0.0	0.66±0.01	0.433±0.001	0.0

Table A2. Estimates of Model Parameter values (*C*), corresponding lower (*L*) and upper (*U*) limits identifying 95% confidence limits (in parenthesis) and value of $\Re = (U - L) / C$ associated with water relative permeability (K_{rw}).

		Sand-pack		Berea sandstone		D1		D2	
Model	Parameter	$\Re$	*C*	$\Re$	*C*	$\Re$	*C*	$\Re$	*C*
Corey	N_w	5.92(4.9;6.8)	.31	0.95(0.69;1.2)	.06	3.31 (2.9;3.7)	.24	2.2(2.1;2.3)	.11
Chierici	*B*	3.21(3.03;4.5)	.47	0.84(0.8;0.9)	.10	2.94 (2.7;3.5)	.27	1.59(1.16;2.01)	.52
Chierici	*M*	0.66(0.62;0.70)	.12	1.62(1.17;2.2)	.64	1.12 (1.03;1.2)	.14	0.88(0.66;1.14)	.61
ET	L_w	4.02(2.71;5.32)	.68	2.14(1.7;2.6)	0.41	3.54 (2.4;4.7)	.66	1.84(1.04;2.6)	.86
ET	E_w	2.00 (0.73;3.28)	.27	0.76(0.52;1.02)	0.63	2.63 (0.3;4.9)	.78	2.28(0.71;3.83)	.37
ET	T_w	0.41(0.27;0.55)	.68	2.59(2.18;3.01)	0.31	1.16 (0.8;1.5)	.60	1.09(0.77;1.40)	.58

Table A3. Estimates of Model Parameter values (C), corresponding lower (L) and upper (U) limits identifying 95% confidence limits (in parenthesis) and value of $\Re = (U - L) / C$ associated with oil relative permeability (K_{ro}).

		Sand-pack		Berea sandstone		D1		D2	
Model	Parameter	C	$\Re$	C	$\Re$	C	$\Re$	C	$\Re$
Corey	N_o	1.02 (0.99;1.05)	.06	2.18 (1.8;2.6)	.37	2.05 (1.67;2.43)	.04	3.95 (3.86;4.40)	.16
Chierici	A	0.67 (0.62;0.73)	.16	1.27 (1.11;1.44)	.26	1.54 (1.46;1.62)	0.07	2.90 (2.78;3.01)	.10
Chierici	L	0.64 (0.53;0.76)	.36	1.35 (0.89;1.81)	.68	1.40 (1.28;1.52)	0.05	0.89 (0.88;0.92)	.17
LET	L_o	1.00 (0.79;1.22)	.43	3.31 (3.08;3.54)	.41	3.11 (2.5;3.72)	.09	4.28 (4.08;4.49)	.39
LET	E_o	1.18 (0.70;1.65)	.80	1.36 (1.14;1.59)	.63	1.60 (0.48;2.74)	.29	1.36 (1.15;1.56)	.40
LET	T_o	1.28 (0.91;1.64)	.57	2.39 (0.58;4.29)	.51	1.83 (1.45;2.22)	.15	0.66 (0.61;0.71)	.42

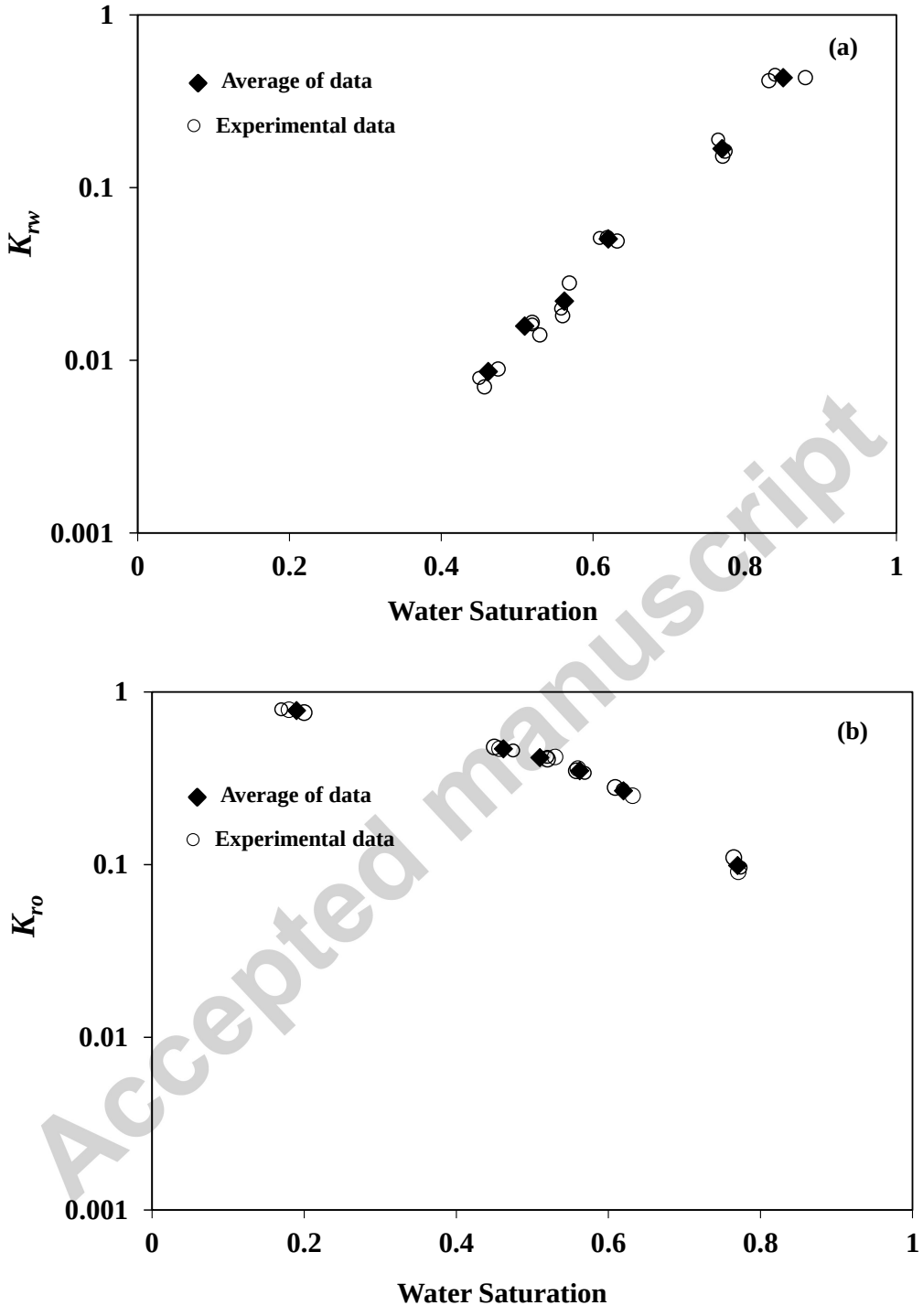

Fig. A1. Steady-State imbibition relative permeabilities (a) K_{rw} and (b) K_{ro} versus water saturation for the Sand-pack experiments.

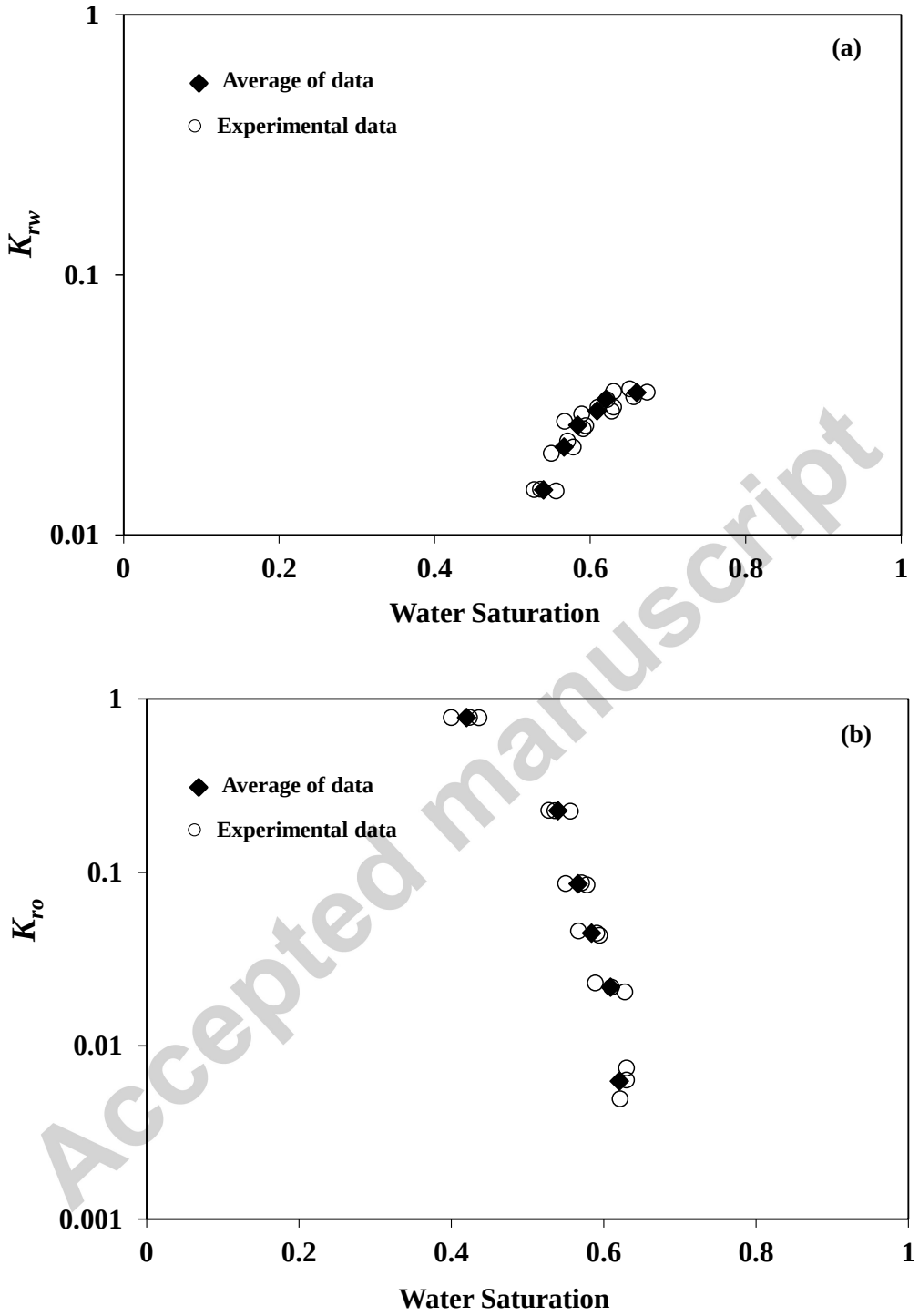

Fig. A2. Steady-State imbibition relative permeabilities (a) K_{rw} and (b) K_{ro} versus water saturation for the Berea sandstone experiments.

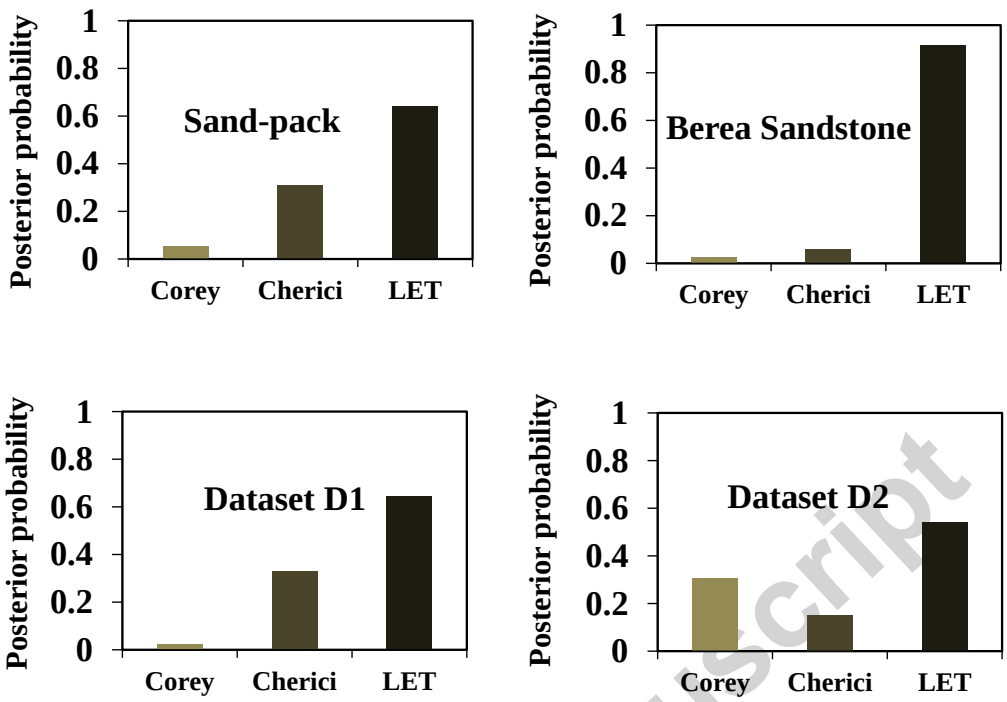

Fig. A3. Posterior probabilities associated with the models tested based on *KIC* and on K_{rw} data interpretation.

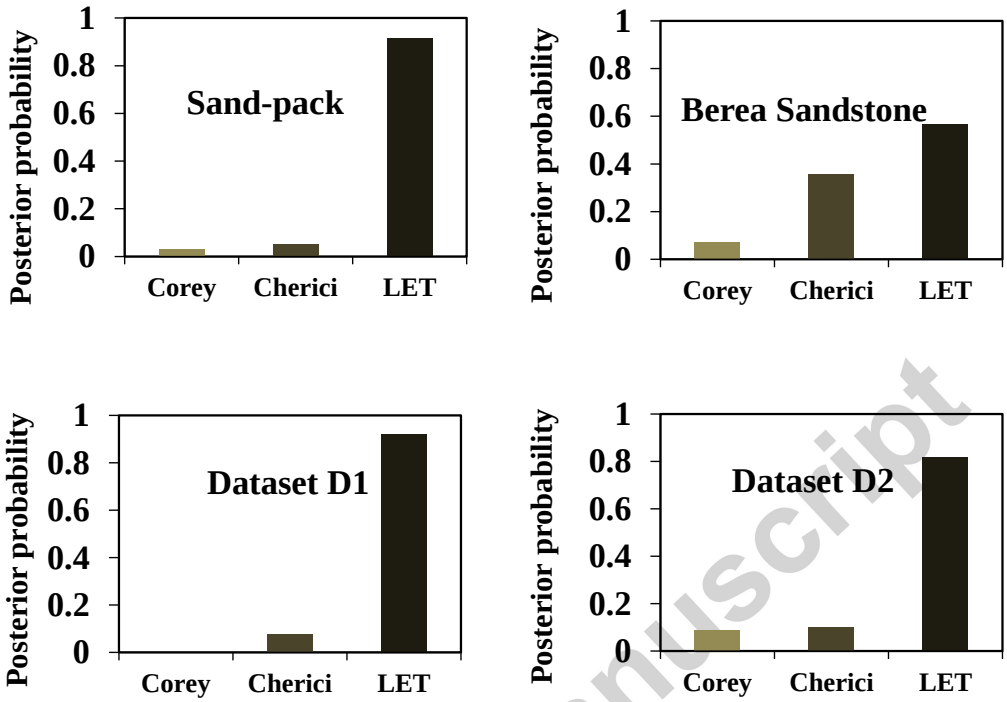

Fig. A4. Posterior probabilities associated with the models tested based on *KIC* and on K_{ro} data interpretation.

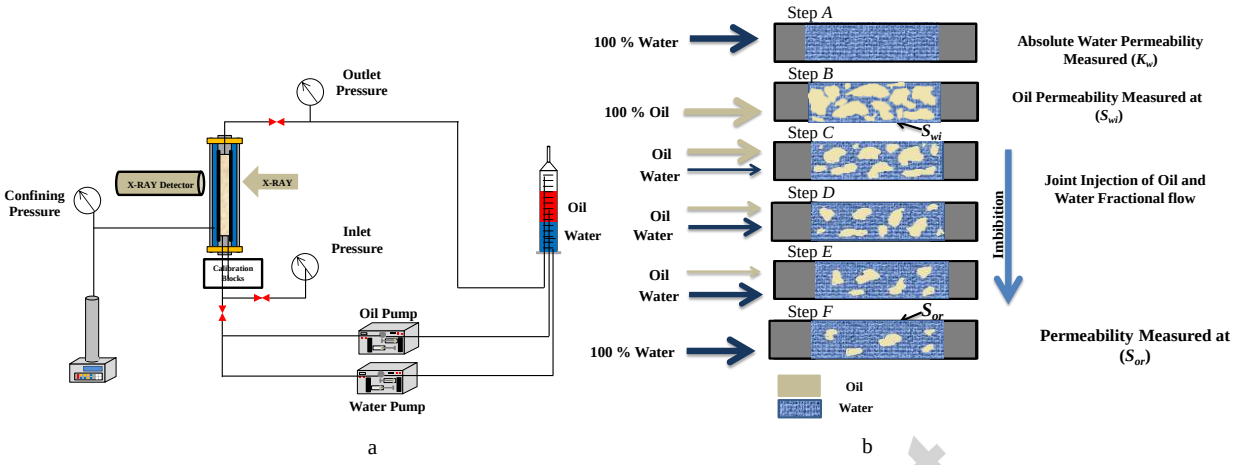

Fig. 1. (a) Sketch of experimental set-up; (b) Steady State (SS) imbibition process.

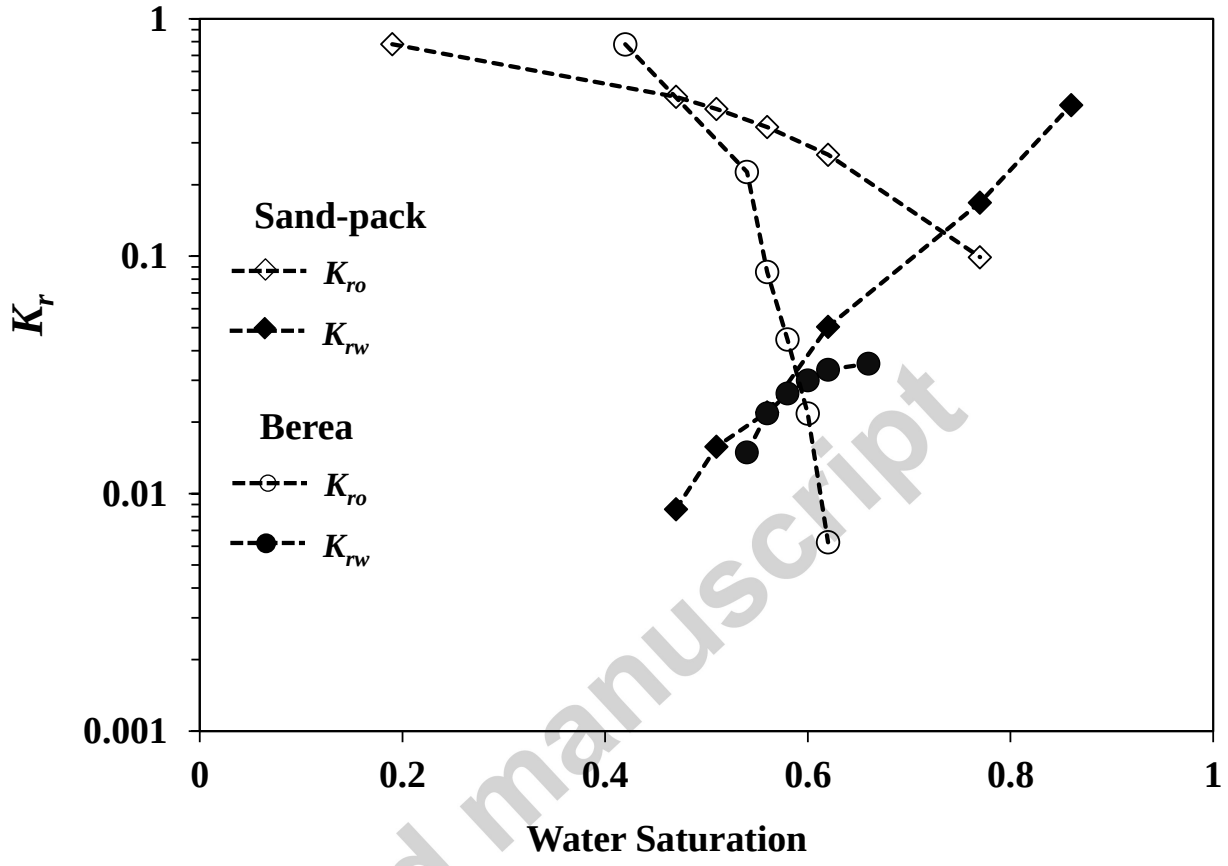

Fig. 2. Steady-State Imbibition relative permeabilities versus average water saturation.

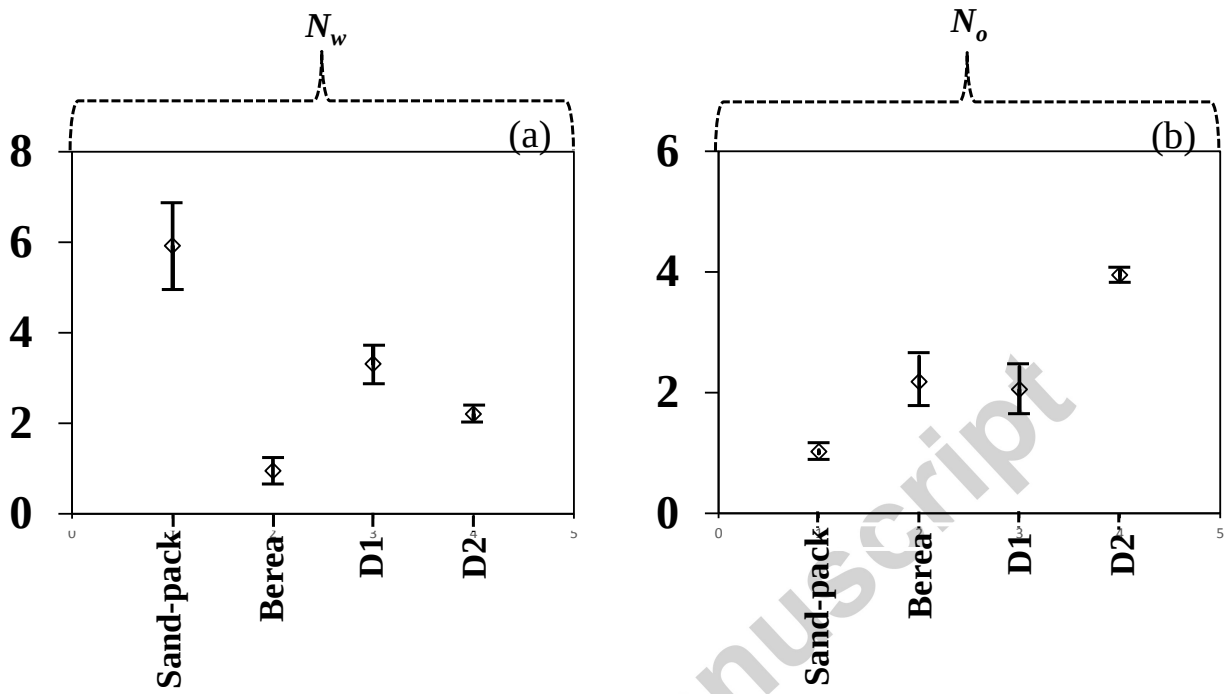

Fig. 3. Estimated Corey model parameter values for (a) K_{rw} and (b) K_{ro} associated with the four considered datasets. Intervals associated with the upper (U) and lower (L) limits identifying the 95% uncertainty bounds around the estimate are also depicted.

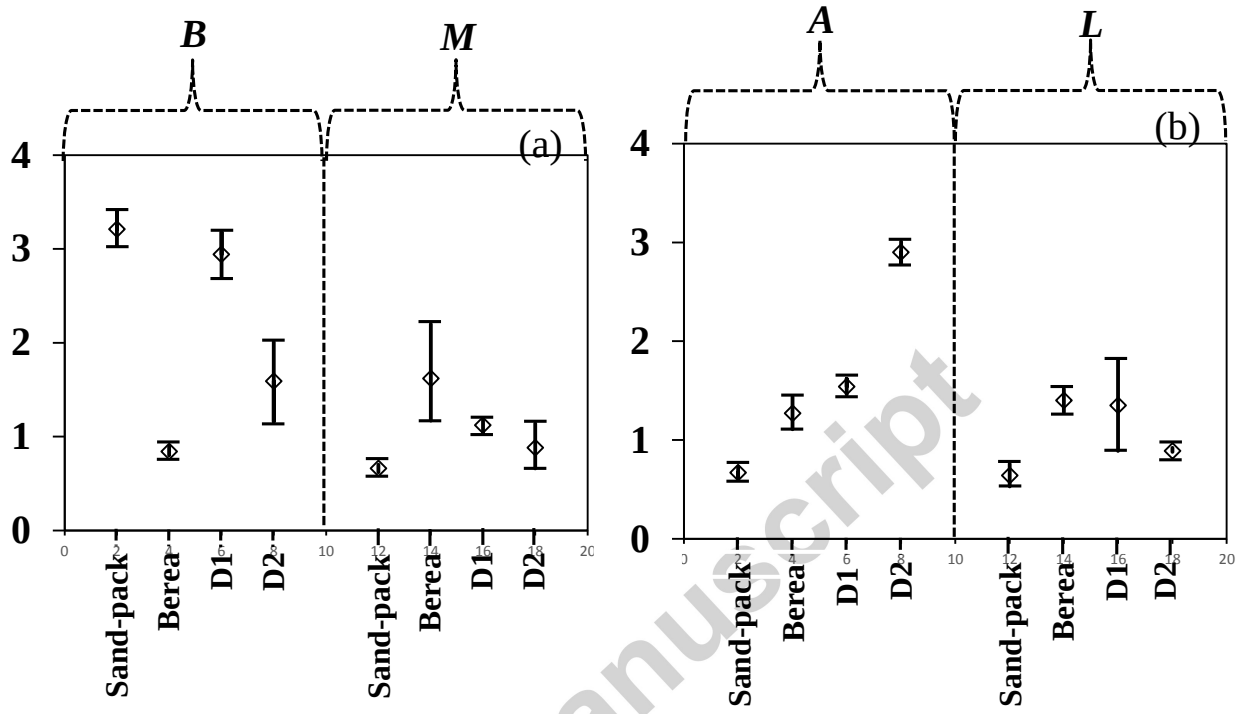

Fig. 4. Estimated Chierici model parameter values for (a) K_{rw} and (b) K_{ro} associated with the four considered datasets. Intervals associated with the upper (U) and lower (L) limits identifying the 95% uncertainty bounds around the estimate are also depicted.

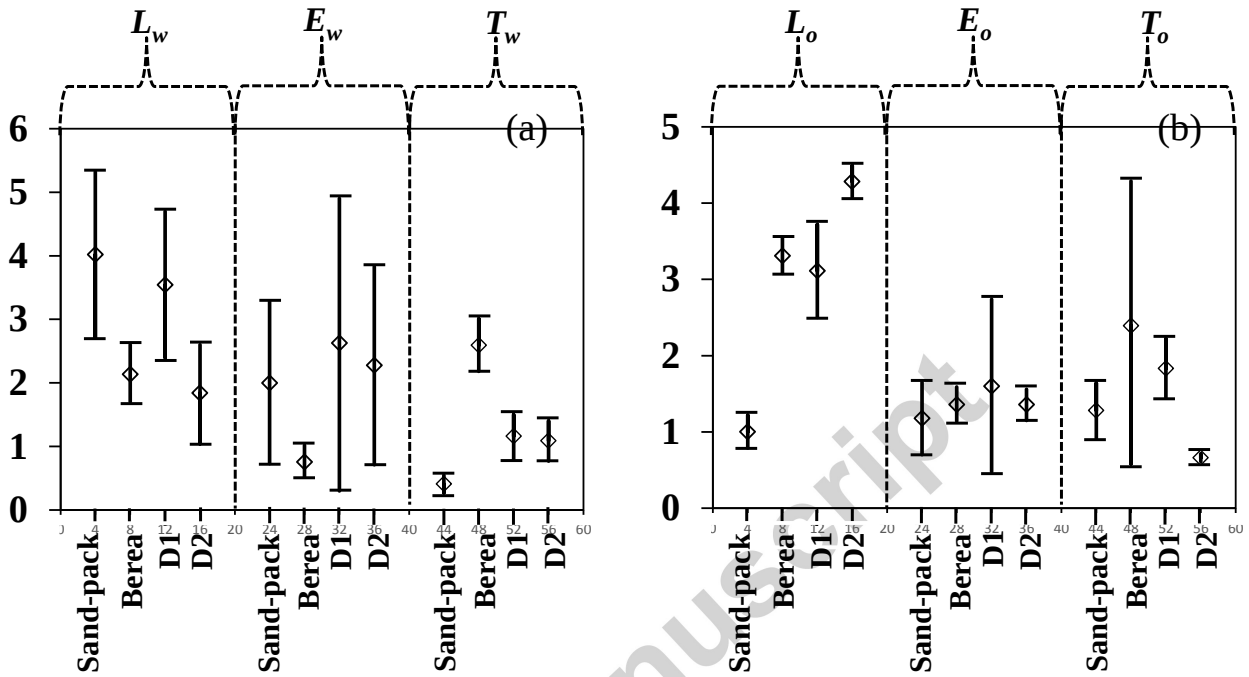

Fig. 5. Estimated LET model parameter values for (a) K_{rw} and (b) K_{ro} associated with the four considered datasets. Intervals associated with the upper (U) and lower (L) limits identifying the 95% uncertainty bounds around the estimate are also depicted.

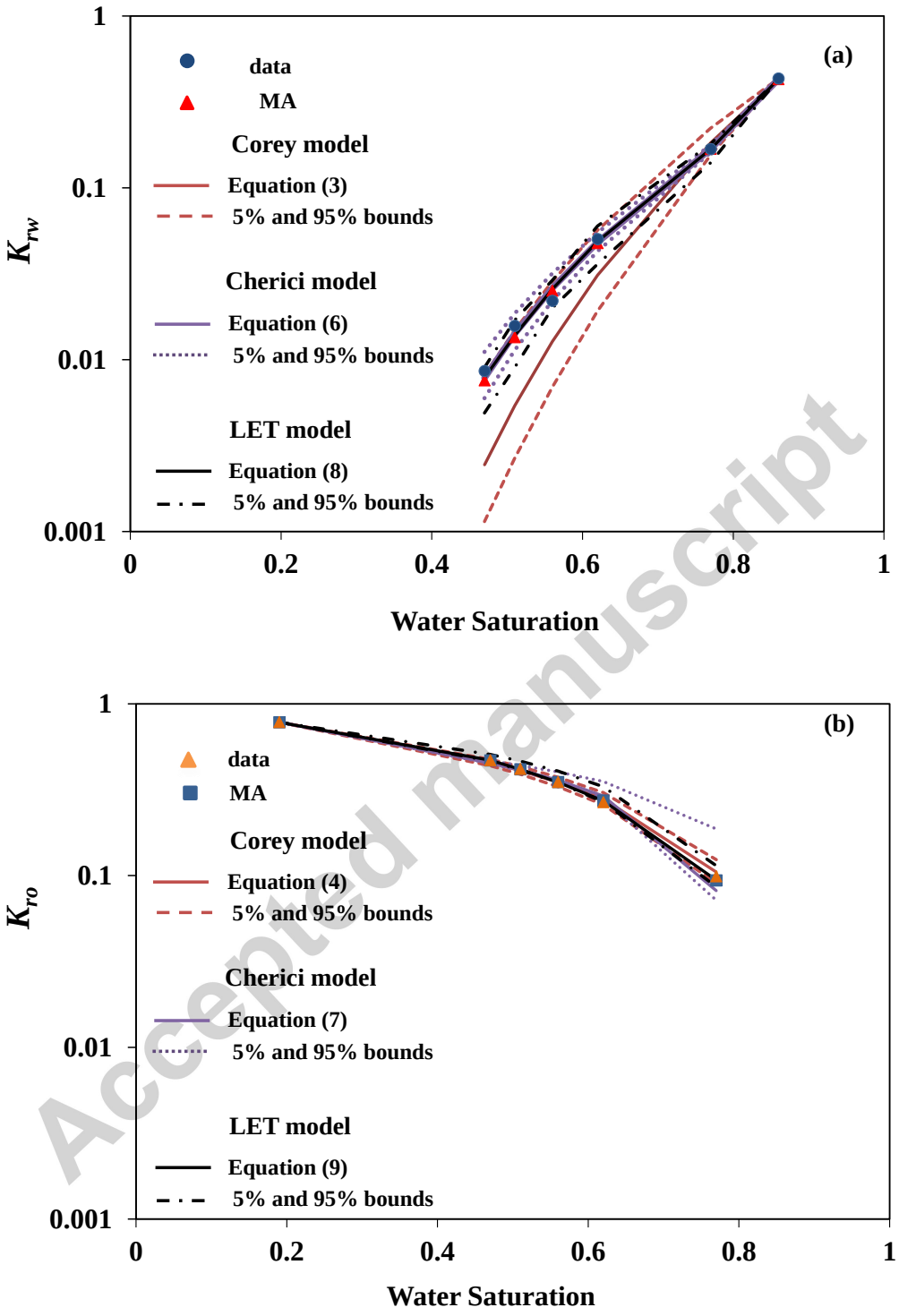

Fig. 6. Graphical depictions of (a) K_{rw}, (b) K_{ro} versus water saturation for the Sand-pack experiments together with the results of all calibrated models, uncertainty bounds corresponding to Gaussian 95% confidence intervals and model average (MA).

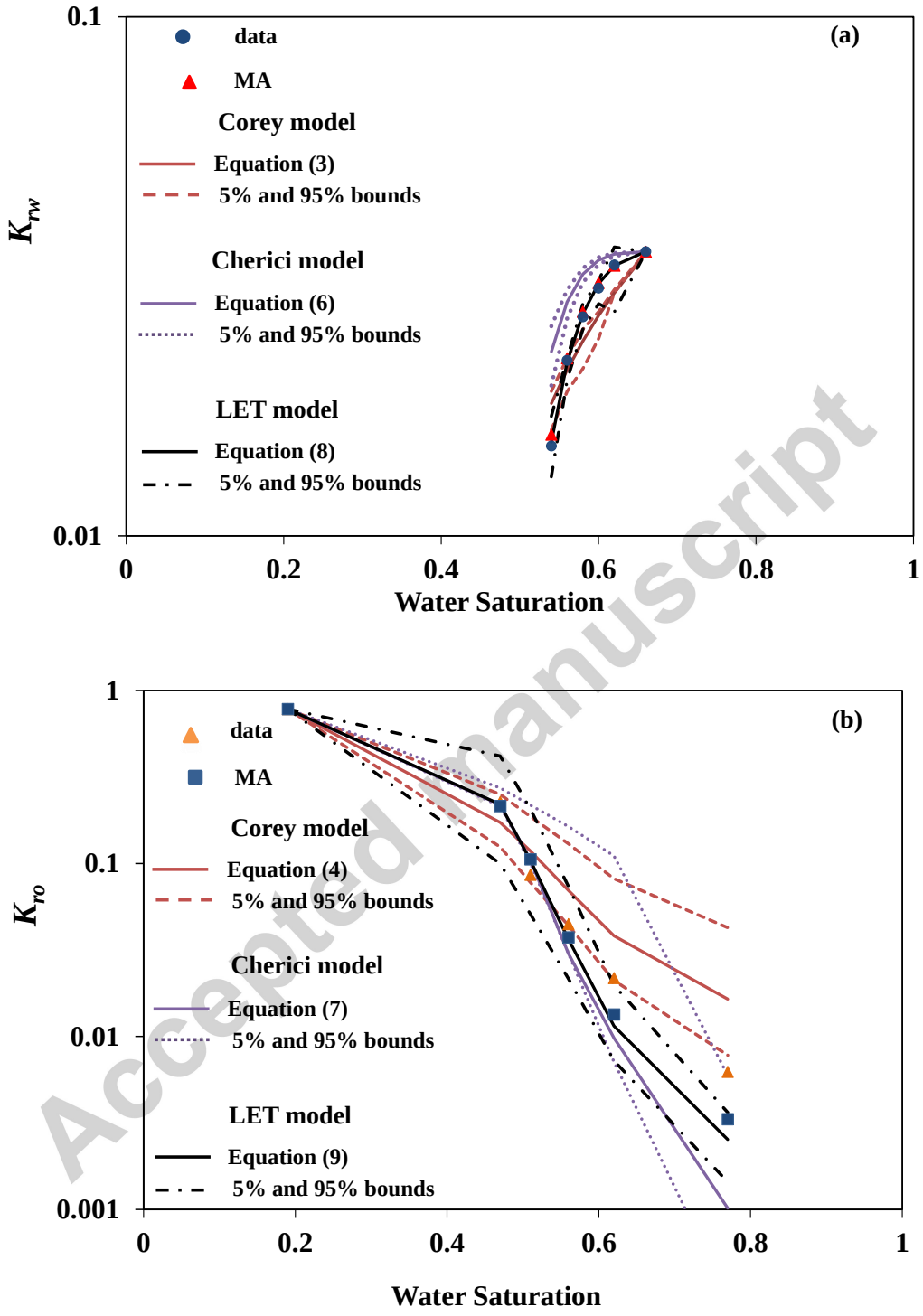

Fig. 7. Graphical depictions of (a) K_{rw}, (b) K_{ro} versus water saturation for the Berea sandstone experiments together with the results of all calibrated models, uncertainty bounds corresponding to Gaussian 95% confidence intervals and model average (MA).

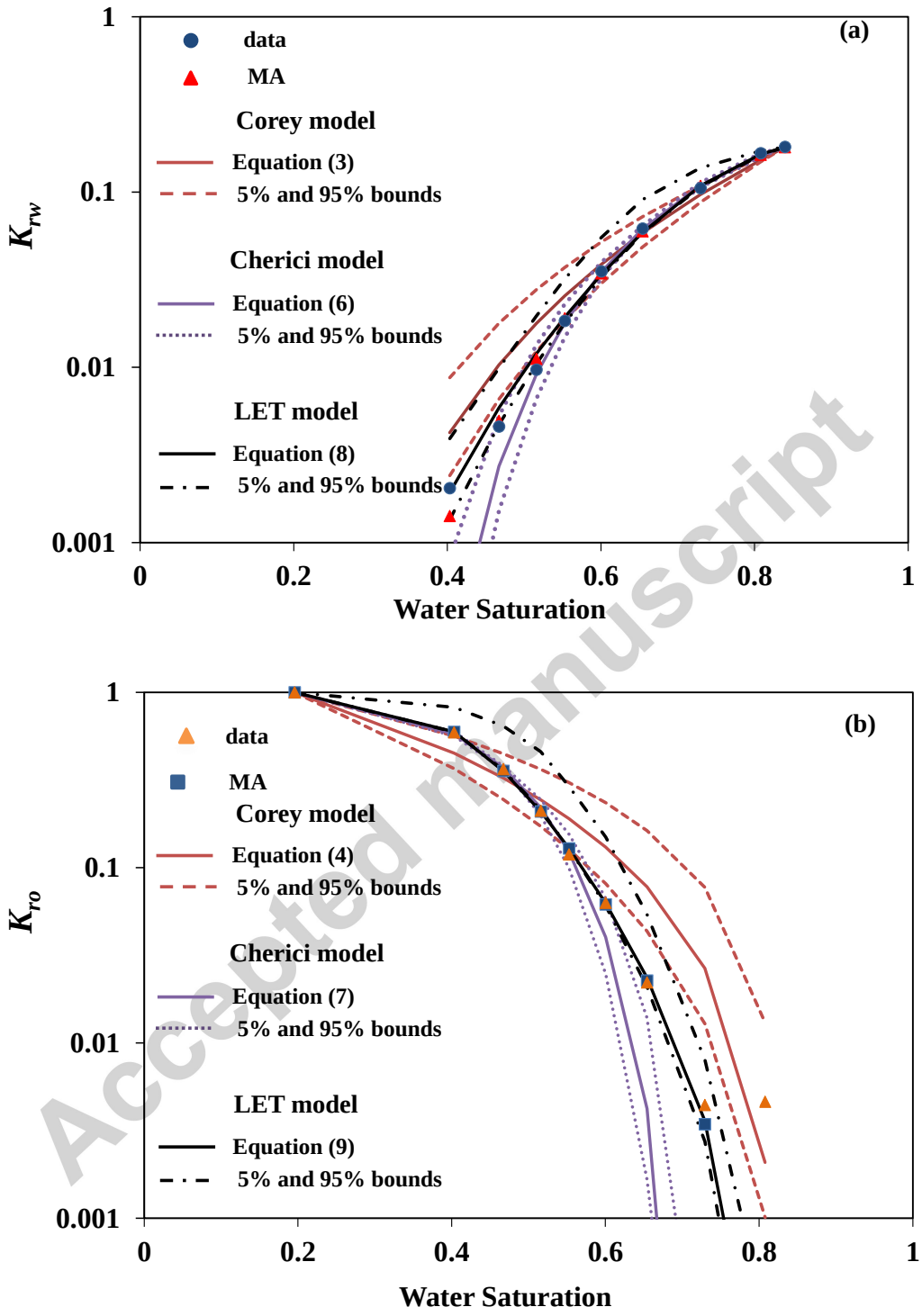

Fig. 8. Graphical depictions of (a) K_{rw}, (b) K_{ro} versus water saturation for dataset D1 together with the results of all calibrated models, uncertainty bounds corresponding to Gaussian 95% confidence intervals and model average (MA).

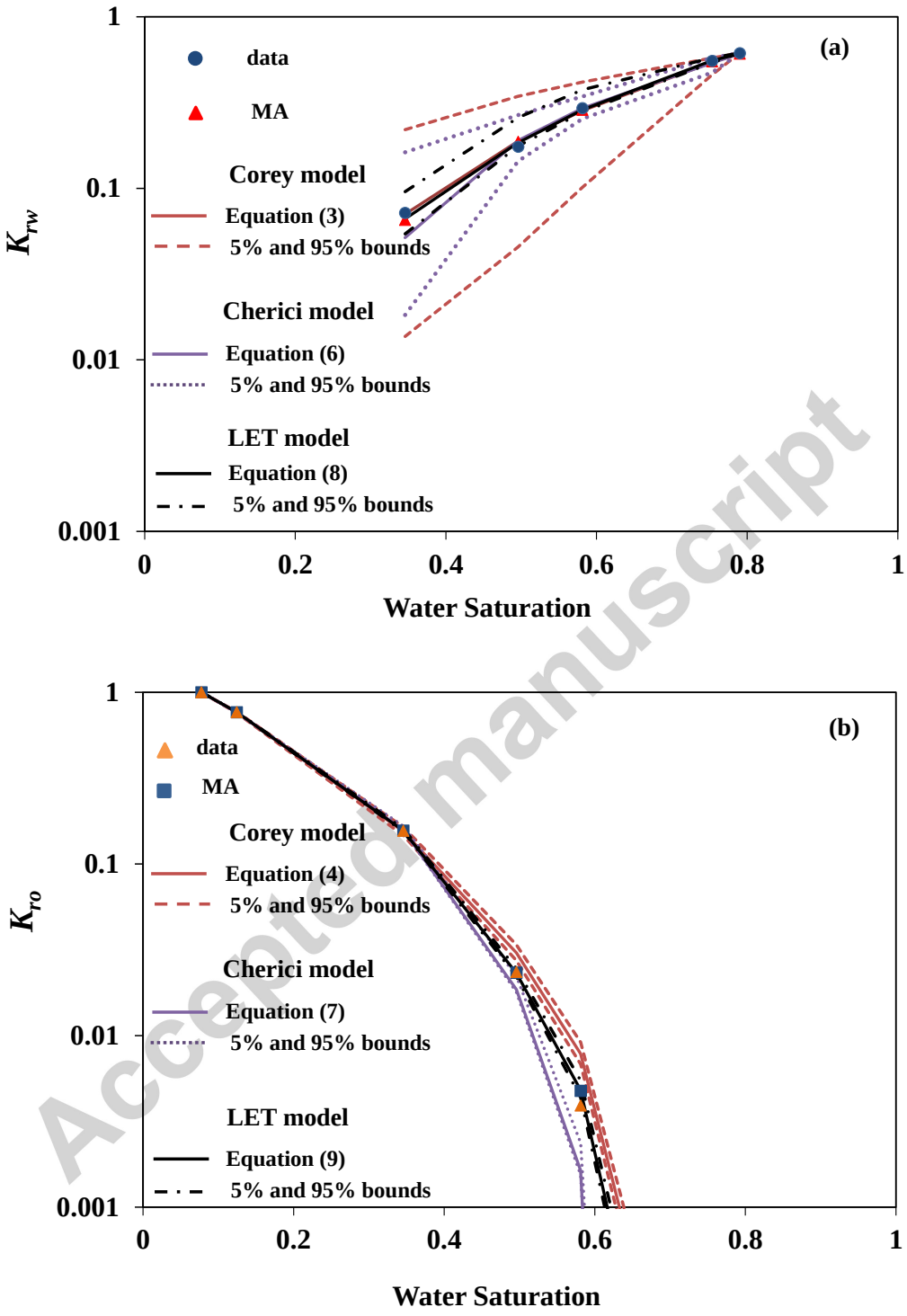

Fig. 9. Graphical depictions of (a) K_{rw}, (b) K_{ro} versus water saturation for dataset D2 together with the results of all calibrated models and uncertainty bounds corresponding to Gaussian 95% confidence intervals and model average (MA).

Highlights:

- We perform high quality steady-state two-phase relative permeability measurements.
- We illustrate the formal model identification criteria to rank and evaluate a set of alternative models.
- We compare the performance of a model averaging approach with skill of each individual model.
- Comparison have been carried out on the basis of the Normalized Mahalanobis Distance and mean square error.
- The results show that model averaged tend to produce high fidelity representations of the observations.

Table 1. Physical properties of the tested core samples and fluids.

	Sand-pack	Bera
Oil viscosity [cP]	1.74	1.74
Water viscosity [cP]	0.97	1.03
Temperature during test [$^{\circ}C$]	25	25
Porosity [%]	37	17
Water absolute permeability [mD]	2900	30
Permeability of oil at S_{wi} [mD]	2500	25

Table 2. Physical properties of Norwegian Continental Shelf core samples and fluids for experiments D1 and D2 (Lomeland et al. 2005)).

	D1	D2
Oil viscosity [cP]	2.41	0.67
Water viscosity [cP]	0.39	0.30
Temperature for test [$^{\circ}C$]	84	95
Porosity [%]	29	27
S_{wi} [-]	0.19	0.07
Permeability of oil at S_{wi} [mD]	2396	1042

Table 3. Model Calibration and Identification Criteria and Corresponding Posterior Probability (in parenthesis) associated with K_{rw} (the smallest values for each dataset are highlighted in bold).

Subsets	*AIC*	*AICc*	*BIC*	*KIC*
Corey				
Sand-pack	-59(0.02)	-56.24(0.04)	-59.39(0.02)	-62.99(0.05)
Berea	-67(0.017)	-62.83(0.14)	-67.24(0.02)	-67.96(0.025)
D1	-96(0.014)	-94.23(0.027)	-95.34(0.015)	-98.23(0.024)
D2	-64(0.37)	**-61.37**(0.83)	-64.48(0.39)	-60.9(0.30)
Chierici				
Sand-pack	**-79**(0.54)	**-71.60**(0.84)	**-79.76**(0.55)	-73.76(0.31)
Berea	-75(0.06)	-67.01(0.29)	-75.17(0.06)	-81.04(0.58)

D 1	-117(0.49)	**-113.12**(0.64)	- **116.2**(0.50)	- 113.98(0.33)
D 2	-57(0.012)	-49.02(0.11)	- 57.18(0.12)	- 56.69(0.15)
LET				
Sand-pack	-78(0.44)	-58.49 (0.09)	- 78.74(0.47)	- **76.18**(0.64)
Berea	**-91**(0.92)	**-71.04**(0.56)	- **91.25**(0.92)	- **89.48**(0.92)
D 1	**-117.3**(0.5)	-109.3(0.33)	- 116.06(0.49)	- **118.02**(0.65)
D 2	**-66**(0.51)	-45.67(0.061)	- **65.9**(0.49)	- **64.31**(0.54)

Table 4. Model Calibration and Identification Criteria and Corresponding Posterior Probability (in parenthesis) associated with K_{ro} (the smallest values for each dataset are highlighted in bold)

Subsets	*AIC*	*AICc*	*BIC*	*KIC*
Corey				
Sand-pack	-63.2 (0.12)	-**60.22**(0.65)	-63.33(0.11)	-58.87(0.032)
Berea	-46.81(0.08)	-43.81(0.30)	-46.91(0.083)	-48.71(0.07)
D1	-52(0.0002)	-50(0.0005)	-51(0.0002)	-54.42(0.001)
D2	-76.6(0.017)	-73.58(0.19)	-76.68(0.016)	-71.23(0.085)
Chierici				
Sand-pack	-54.4(0.03)	-46.38(0.06)	-54.54(0.02)	-49.22(0.05)
Berea	-55.78(0.37)	-**47.8**(0.58)	-55.95(0.37)	-55.38(0.36)
	-84.7(0.042)	-	-	-

D1			80(0.0789)	83.78(0.043)	80.82(0.08)
		-79(0.025)	-	-	-
D2			71.6(0.14)	79.8(0.03)	71.85(0.10)
LET					
		-75.1(0.85)	-	-	-
Sand-pack			55.08(0.28)	**75.29**(0.85)	**66.67**(0.92)
		-57.97(0.54)	-	-	-
Berea			37.97(0.11)	**58.18**(0.54)	**58.72**(0.57)
	D1	**-103.**5(0.96)	-	-	-
			95.53(0.92)	**102.32**(0.96)	**98.74**(0.92)
	D2	**-101**(0.96)	-	-	-
			81.03(0.68)	**101.25**(0.96)	**84.57**(0.82)

Table 5. Average Mahalanobis distance (NMD_m), standard deviation of *NMD* (*SDNMD*), the resulting coefficient of variation ($CV = SDNMD / NMD_m$) and Mean Square Error (*MSE*) for each model of the population considered and its MA based counterpart for K_{rw}.

	Sand-pack				Berea				D1				D2			
	$DNMD_m$	MD_m	V	SE	$DNMD_m$	MD_m	V	SE	$DNMD_m$	MD_m	V	SE	$DNMD_m$	MD_m	V	SE
orey	.42	.79	.51	.35E-04	.27	.9	.16	.40E-06	.97	.57	.21	.45E-05	.55	.1	.26	.90E-05
hierici	.44	.85	.51	.40E-05	.17	.82	.15	.14E-05	.99	.45	.22	.47E-06	.61	.1	.29	.72E-04
LET	.44	.84	.51	.00E-05	.21	.92	.15	.30E-08	.01	.46	.23	.06E-06	.56	.1	.27	.07E-05
A	.44	.84	.51	.36E-05	.21	.93	.15	.07E-07		.46	.22	.06E-06	.56	.1	.27	.06E-05

Table 6. Average Mahalanobis distance (NMD_m), standard deviation of *NMD* (*SDNMD*), the resulting coefficient of variation ($CV = SDNMD / NMD_m$) and Mean Square Error (*MSE*) for each model of the population considered and its MA based counterpart for K_{ro}.

	Sand-pack				Berea				D1				D2			
	$DNMD_m$	MD_m	V	SE	$DNMD_m$	MD_m	V	SE	$DNMD_m$	MD_m	V	SE	$DNMD_m$	MD_m	V	SE
orey	.04	.84	.56	.80E-04	.74	.71	.01	.04E-04	.65	.42	.11	.60E-03	.99	.88	.13	.00E-06
hierici	.04	.86	.56	.0013	.72	.66	.03	.14E-04	.59	.32	.21	.15E-04	.99	.87	.14	.90E-06
ET	.03		.51	.90E-05	.71	.65	.02	.10E-05	.58	.31	.21	.32E-05	.99	.87	.14	.72E-07
A	.03		.51	.80E-05	.72	.67	.02	.37E-05	.59	.32	.21	.04E-05	.99	.87	.14	.06E-08